

# PARTIAL DIFFERENTIAL EQUATIONS IN IMAGE ANALYSIS: CONTINUOUS MODELING, DISCRETE PROCESSING \*

PETROS MARAGOS

School of E.C.E., Georgia Institute of Technology, Atlanta, GA 30332, U.S.A.  
Institute for Language & Speech Processing, Artemidos/Epidavrou Str., Marousi 15125, Greece.  
e-mail: maragos@ee.gatech.edu

## ABSTRACT

This paper presents an overview of selected topics from an emerging new image analysis methodology that starts from continuous models provided by partial differential equations (PDEs) and proceeds with discrete processing of the image data via the numerical implementation of these PDEs on some discrete grid. We briefly discuss basic ideas, examples, algorithms, and applications for PDEs modeling nonlinear multiscale analysis, geometric evolution of curves and signals, nonlinear image/signal restoration via shock filtering, and the eikonal PDE of optics. Wherever possible, we compare the PDE approach with the corresponding all-discrete method. The PDE approach is very promising for solving (or improving previous all-discrete solutions of) many problems in image processing and computer vision because it provides new and more intuitive mathematical models, has connections with physics, gives better approximations to the Euclidean geometry of the problem, and is supported by efficient discrete numerical algorithms based on difference approximations.

## 1 Introduction

Digital image processing has been based traditionally on the basic principles of digital processing of signals, which dictate sampling the signal and then doing both the modeling and processing in the discrete domain. Examples include the 2D ARMA models via linear difference equations, the 2D nonlinear difference equations of the max/min/rank type involved in morphological/rank filtering, the 2D Markov models, and the 2D discrete transforms (e.g., DFT or DCT). In one exception [20] continuous models, i.e., linear *partial differential equations (PDEs)* were used to better represent discrete random images and model their covariances.

In contrast to the all-discrete approaches which dominated image processing, in computer vision there have been proposed continuous models for several vision tasks based on PDEs. The discrete part of such approaches comes only in the corresponding difference equations that approximate the solution of these PDEs. Motivations for using PDEs include better and more intuitive mathematical modeling,

\* Part of this work was done at Georgia Tech and was supported by the US NSF under grant MIP-94-21677 and by the ARO under grant DAAH04-96-1-0161. Another part was done and the paper was written while P. Maragos was at I.L.S.P. It was also partially supported by the European TMR/Networks Project ERBFMRXCT970160.

connections with physics, and better approximation to the Euclidean geometry of the problem. While many such continuous approaches have been linear, the majority and the most useful ones are nonlinear, which is partly due to a general understanding in image processing about the limitations or inability of linear systems to successfully model several important problems and hence about the need to develop nonlinear approaches.

One major effort [18] was the use of PDEs in problems of shape from shading and optical flow computation. However, the most well known vision problem modeled via PDEs is that of multiscale analysis, which is a useful and often required framework for many tasks such as feature/object detection, motion detection, stereo, and multi-band frequency analysis. Consider a multiscale operator  $\mathcal{T}_t$  mapping an input image  $f$  to an output image  $\mathcal{T}_t(f)$  which results from the (linear or nonlinear) interaction of  $f$  with some kernel function dependent on a continuous scale parameter  $t \geq 0$ :

$$u(x, y, 0) = f(x, y) \longrightarrow [\mathcal{T}_t] \longrightarrow \mathcal{T}_t(f)(x, y) = u(x, y, t)$$

The scale-space function  $u(x, y, t)$  holds all the history of transforming  $f$  through all scales. From the operator viewpoint,  $u$  can be viewed as the output of  $\mathcal{T}_t$  at any fixed scale  $t$ . From an alternative viewpoint, *evolution PDEs* of the type<sup>1</sup>

$$u_t = \text{function}(u_{xx}, u_{xy}, u_{yy}, u_x, u_y, u, x, y, t)$$

have been developed to model the evolution of  $u$  in scale-space as a continuous dynamical system and view  $u$  as the solution to the initial-value problem of the above PDE with  $u(x, y, 0) = f(x, y)$ . The PDE approach is more general and useful; sometimes it is also the only possibility because only in special cases the multiscale operator  $\mathcal{T}_t$  has a closed-formula expression as some operation on  $f$ . The earliest and most well-known PDE example is the linear heat-diffusion PDE [24] for modeling the Gaussian scale-space [32, 55]. Dissatisfaction with the edge blurring and shifting of this linear scale-space motivated the development of anisotropic nonlinear diffusion PDEs for multiscale directional image smoothing and edge detection [41, 11, 2]. Edge sharpening and contrast enhancement has also been modeled in [39, 3] by nonlinear wave PDEs that can generate shocks [25]. Independently from the Gaussian scale-space ideas and their

<sup>1</sup>Notation:  $u_t = \partial u / \partial t$ ,  $u_x = \partial u / \partial x$ ,  $u_y = \partial u / \partial y$ ,  $\nabla u = (u_x, u_y)$ ,  $\text{div}((v, w)) = \nabla \cdot (v, w) = v_x + w_y$ .

anisotropic/nonlinear improvements, there pre-existed nonlinear filters of the morphological type that can smooth while preserving important image features and can create a nonlinear scale-space [33, 49, 28]. In [1, 8, 51, 9, 52] nonlinear PDEs were developed to model multiscale morphological dilations/erosions. These morphological PDEs are related to broader classes of nonlinear PDEs that can model nonlinear dynamics in image processing. For references see [4] and the papers in [19]. For example, representing multiscale morphology via distance transforms and interpreting distance propagation as wave propagation leads to an important nonlinear PDE, the eikonal equation [7, 48] of optics. This ubiquitous PDE has been applied to solving various problems in image analysis and computer vision such as gridless halftoning, image segmentation, and shape-from-shading [18, 53, 44, 48, 42, 23, 36, 38, 29, 30].

In parallel to the development of the above ideas, there have been some advances in differential geometry for evolving curves or surfaces using level set methods. Specifically, nonlinear PDEs of the Hamilton-Jacobi type were developed in [40, 50] to model the propagation of curves embedded as level sets of functions evolving in scale-space, using curvature-dependent speeds normal to the curve. These PDEs of curve evolution contain the PDE of multiscale morphological dilation by disks as a basic ingredient [46]. Curve evolution has been applied to model and solve a large variety of problems in image analysis and computer vision [50, 21]. Its success is largely due to the development [40, 50] of stable and shock-capturing discretization schemes to numerically solve the resulting PDEs.

In this paper we briefly discuss the above ideas as well as the numerical implementation and applications of some selected nonlinear PDEs. Wherever possible, we also compare the PDE approach with the corresponding all-discrete method.

## 2 Gaussian Scale-Space, Heat-Diffusion PDE

Following the biologically-motivated in [32] formulation of many information extraction tasks in vision as a multiscale image analysis problem using linear Gaussian convolutions, two other important developments were the continuous Gaussian scale-space [55] and the observation in [24] that this can be modeled via the heat diffusion equation. Specifically, if

$$u(x, y, t) = f * G^{(t)} \quad , \quad G^{(t)}(x, y) \equiv \exp[-(x^2 + y^2)/4t]/4\pi t,$$

is the linear convolution  $*$  of an image  $f$  by a 2D Gaussian  $G^{(t)}$  at scale  $t \geq 0$  (here ‘scale’ is proportional to the variance  $(2t)$  of  $G^{(t)}$ ), then  $u$  can be generated from the linear heat conduction (or diffusion) PDE as solution to the initial value problem

$$u_t = \nabla^2 u = u_{xx} + u_{yy} \quad , \quad u(x, y, 0) = f(x, y) \quad (1)$$

This diffusion law holds for an isotropic and homogeneous medium. The popularity of this approach is due to its linearity and relations to the heat PDE about which much is known from physics and mathematics. Its big disadvantage is that the (linear low-pass) Gaussian smoothing blurs image edges, which makes their detection and localization difficult. See Fig. 1 to contrast multiscale Gaussian filtering with edge-preserving (nonlinear) morphological filters.

## 3 Multiscale Morphology and Dilation PDEs

The main tools of morphological image processing are a broad class of nonlinear signal operators formed as parallel and/or serial interconnections of the two most elementary morphological signals operators, the *dilation*  $f \oplus g$  and the *erosion*  $f \ominus g$  of an input signal  $f$  by a structuring function  $g$ . Compositions of erosions and dilations yield two useful smoothing filters: the *opening*  $f \mapsto (f \ominus g) \oplus g$  and *closing*  $f \mapsto (f \oplus g) \ominus g$ . The above morphological signal operations and their combinations have found a broad range of applications in image processing and computer vision; see [49, 31] for surveys and references. Multiscale morphological operations are particularly useful for nonlinear multiscale smoothing, size distributions, geometrical feature extraction, shape analysis, and segmentation [33, 49, 28, 31, 45]. They are obtained by replacing in the dilations/erosions the unit-scale kernel  $g$  with a multiscale function  $g^{(t)}(x, y) \equiv tg(x/t, y/t)$ ,  $t > 0$ . Thus, the *multiscale dilation* of  $f$  by  $g^{(t)}$  is the space-scale function

$$u(x, y, t) \equiv (f \oplus g^{(t)})(x, y) = \sup_{(a,b)} \{f(x-a, y-b) + tg(a/t, b/t)\}$$

where  $u(x, y, 0) = f(x, y)$ . In practice, a useful class of functions  $g$  are defined as the supports of convex planar sets  $B \equiv \{(x, y) \in \mathbb{R}^2 : \|(x, y)\|_p \leq 1\}$  that are the unit balls of the metrics induced by the  $L_p$  norms  $\|\cdot\|_p$  for  $p = 1, 2, \dots, \infty$ . The corresponding flat structuring functions are  $g(x, y) = 0$  if  $(x, y) \in B$  and  $-\infty$  else. The PDEs generating the multiscale dilations of  $f(x, y)$  by the above flat structuring elements  $B$  are [9, 4]

$$u_t = \sup_{\|(a,b)\|_p \leq 1} au_x + bu_y = \|\nabla u\|_q \quad , \quad \frac{1}{p} + \frac{1}{q} = 1 \quad (2)$$

For example, if  $p = q = 2$ ,  $B$  is the unit disk,  $\|\cdot\|_2 = \|\cdot\|$  is the Euclidean norm and

$$u_t = \|\nabla u\| = \sqrt{(u_x)^2 + (u_y)^2} \quad (3)$$

These simple but nonlinear PDEs are satisfied at points where the data are smooth, i.e., the partial derivatives exist. However, even if the initial image/signal  $f$  is smooth, at finite scales  $t > 0$  the above multiscale dilation evolution may create discontinuities in the derivatives of  $u$ , called *shocks*, which then continue propagating in scale-space. Thus, the multiscale dilations are *weak solutions* of the corresponding PDEs. Ways to deal with these shocks include replacing standard derivatives with morphological sup/inf derivatives [9, 29] or replacing the PDEs with differential inclusions [34].

The above PDEs for dilations of graylevel images by flat structuring elements directly apply to binary images, because flat dilations commute with thresholding and hence, when the graylevel image is dilated, each one of its thresholded versions representing a binary image is simultaneously dilated by the same element and at the same scale. However, this is not the case with graylevel structuring functions. We provide two examples of PDEs generating multiscale dilations by graylevel structuring functions: If  $g$  is the compact-support spherical function  $g(x, y) = \sqrt{1 + x^2 + y^2}$  if  $x^2 + y^2 \leq 1$  and  $-\infty$  else, the dilation PDE becomes [9, 52]

$$u_t = \sqrt{1 + (u_x)^2 + (u_y)^2} \quad (4)$$

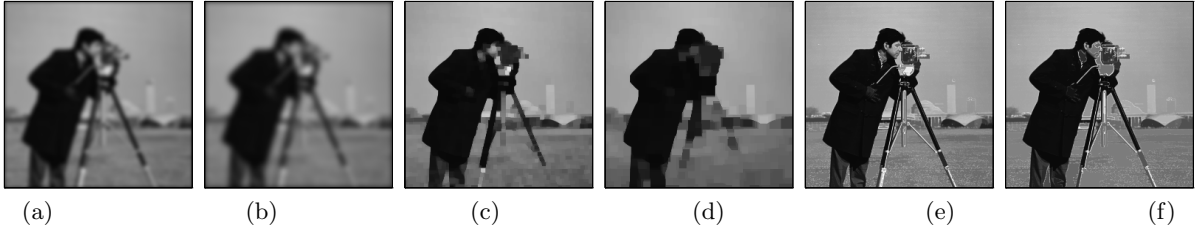


Figure 1: Multiscale smoothings of the CAMERAMAN image at scales  $t = 4$  for Figs. (a,c,e) and  $t = 8$  for Figs. (b,d,f). The smoothers are: (a,b) Linear convolutions with Gaussians of standard deviation  $\sqrt{2t}$ ; (c,d) Morphological clos-opening by a square of  $(t+1) \times (t+1)$  pixels; (e,f) Clos-opening by reconstruction by a square of  $(t+1) \times (t+1)$  pixels.

For the infinite-support parabolic structuring function  $g(x, y) = -0.5(x^2 + y^2)$  the dilation PDE becomes [52]

$$u_t = (u_x)^2 + (u_y)^2 \quad (5)$$

All the above dilation PDEs can be unified by a general formula derived in [17] and stating that, the rate of change of  $u$  in the scale ( $t$ ) direction is equal to the upper slope transform of the structuring function evaluated at the spatial gradient of  $u$ ; i.e.,

$$u_t = \sup_{a,b} \{g(x, y) - ax - bx\}|_{a=u_x, b=u_y} \quad (6)$$

The erosion is a dual operation of dilation and is defined as  $(f \ominus g)(x, y) = \inf_{a,b} \{f(x+a, y+b) - g(a, b)\}$ . The multiscale erosion, i.e., erosion of  $f$  by  $g^{(t)}$  can be generated from PDEs that are exactly the same as the dilation PDEs above but with a ‘−’ sign in front of the right-hand side.

#### 4 Distance Transforms

For binary images, the distance transform is a compact way to represent their multiscale dilations and erosions by compact convex structuring elements whose shape depends upon the norm used to measure distances. Specifically, a binary image  $f(x, y)$  can be divided into the foreground set  $S = \{(x, y) : f(x, y) = 1\}$  and the background set  $S^c = \{(x, y) : f(x, y) = 0\}$ . If  $S \subseteq \mathbb{R}^2$  is used as the domain to measure distances from the background  $S^c$ , its distance transform (also known as its *distance function*) is defined as

$$d_S(x, y) \equiv \inf_{(v,w) \in S^c} \{||(x - v, y - w)||\} \quad (7)$$

The Euclidean norm  $|| \cdot ||$  can also be replaced by other norms, e.g., by any  $L_p$  norm  $|| \cdot ||_p$ . Let  $B \subseteq \mathbb{R}^2$  be the unit ball induced by the norm  $|| \cdot ||_p$ . Then, thresholding the corresponding distance transform at level  $r > 0$  yields the morphological erosion  $\ominus$  of  $S$  by  $B$  of radius (scale)  $r$ : i.e.,  $S \ominus rB = \{(x, y) : d_S(x, y) \geq r\}$  where  $rB = \{(rx, ry) : (x, y) \in B\}$ . Multiscale dilations of  $S$  can be obtained from the distance transform of  $S^c$ .

Using Huygen’s construction [7], the boundaries of multiscale dilations/erosions by disks can also be viewed as the wavefronts of a wave initiating from the original image boundary and propagating with constant normal speed, i.e., in a homogeneous medium. Thus, the distance function has a minimum time-of-arrival interpretation [5] and its isolevel contours coincide with those of the wave phase function. Points where these wavefronts intersect and extinguish themselves (according to the grassfire propagation principle

[5]) are the points of the skeleton (medial) axis of  $S$  [5]. Overall, the Euclidean distance function  $d_S$  is the weak solution of the following nonlinear PDE

$$||\nabla d_S|| = 1 \quad (8)$$

in the interior of  $S$ . This is a special case of the eikonal PDE  $||\nabla \phi|| = \eta$  which corresponds to wave propagation in heterogeneous media and whose solution  $\phi$  is a gray-weighted distance function, where the weights  $\eta(x, y)$  are inversely proportional to the varying propagation speed [26, 53, 44].

In addition to being a compact representation for multiscale erosions and dilations, the distance transform has found many applications in image analysis and computer vision. Examples include skeletonization, size distributions, shape description, object detection and recognition, segmentation. Thus, many algorithms have been developed for its computation on discrete images. To obtain isotropic distance propagation, the *Euclidean distance transform*, i.e., using the Euclidean norm  $|| \cdot ||$  in (7), is desirable because it gives multiscale morphology with the disk as the structuring element. However, it has a significant computational complexity. **Discrete approaches** use various techniques to obtain integer approximations to the Euclidean distance transform at a lower complexity. Notable such examples are the *chamfer metrics* [43, 6], computed by running recursive min-sum difference equations over the image and thus propagating local distances within a neighborhood mask. Their associated unit ball is a polygon whose approximation of the disk improves by increasing the size of the mask and optimizing the local distances. In this paper, for optimal chamfer transforms we shall use the local distances found in [10] by minimizing the max absolute approximation error.

The **continuous approach** to both multiscale morphology and Euclidean distance transforms uses the *dilation PDE* (3) numerically implemented by curve evolution algorithms (explained next). This gives a much better approximation of Euclidean geometry.

#### 5 Curve Evolution

Consider at time  $t = 0$  an initial simple, smooth, closed planar curve  $\gamma(0)$  which is propagated for  $t > 0$  along its normal vector field with speed  $c$ . Let this evolving curve (front)  $\gamma(t)$  be represented by its position vector  $\vec{X}(p, t) = (x(p, t), y(p, t))$  and be parameterized by  $p$  so that it has its interior on the left in the direction of increasing  $p$ . The metric  $||\vec{X}_p|| = \sqrt{x_p^2 + y_p^2}$  is the speed while traveling the curve. If the curve is re-parameterized via its (Euclidean) arc

length parameter  $\ell(p, t) = \int_0^p \|\vec{X}_p(\xi, t)\| d\xi$ , then  $\|\vec{X}_\ell\| = 1$ . The (Euclidean) curvature is

$$\kappa \equiv \frac{\partial \arctan(y_p/x_p)}{\partial \ell} = \frac{y_{pp}x_p - y_p x_{pp}}{(x_p^2 + y_p^2)^{3/2}} \quad (9)$$

A general front propagation law (flow) is

$$\frac{\partial \vec{X}(p, t)}{\partial t} = c \vec{N}(p, t) \quad , \quad \vec{X}(p, 0) = \gamma(0), \quad (10)$$

where  $\vec{N}(p, t)$  is the instantaneous unit *outward normal* vector at points on the evolving curve, and  $c \equiv \vec{X}_t \cdot \vec{N}$  is the *normal speed* function which generally depends on local geometrical information such as the curvature, global image properties, or other factors independent of the curve. If  $c = 1$  or  $c = -1$ , then  $\gamma(t)$  is the dilation or erosion of the initial curve  $\gamma(0)$  by a disk of radius  $t$ .

### 5.1 Eulerian Formulation & Level Set Method

To overcome the topological problem of splitting and merging and numerical problems with the Lagrangian formulation (10), an Eulerian formulation was proposed in [40] where the original curve  $\gamma(0)$  is first embedded in the surface of an arbitrary 2D Lipschitz continuous function  $\psi_0(x, y)$  as its zero level set. (For example, we select  $\psi_0(x, y)$  to be equal to the distance function  $\pm d(x, y)$  from the boundary of  $\gamma(0)$  where + is for points inside and - is for points outside the curve.) Then, the evolving planar curve is *embedded* as the zero level set of an evolving space-time function  $\psi(x, y, t)$ ; this embedding can be expressed in two equivalent ways:

$$\gamma(t) = \{(x, y) : \psi(x, y, t) = 0\} \iff \psi(\vec{P}(t), t) = 0 \quad (11)$$

where  $\vec{P}(t) = \vec{X}(p_0, t)$  is the path of a point on the front. At any point on the front the curvature and outward normal of the level sets can be found from  $\psi$ ; i.e.,

$$\vec{N} = -\frac{\nabla \psi}{\|\nabla \psi\|} \quad , \quad \kappa = -\operatorname{div}\left(\frac{\nabla \psi}{\|\nabla \psi\|}\right) = \nabla \cdot \vec{N} \quad (12)$$

Further, differentiating (11) yields  $\psi_t + \nabla \psi \cdot \vec{P}_t = 0$  which in turn gives the PDE governing the evolution of the embedding function:

$$\psi_t = c \|\nabla \psi\| \quad , \quad \psi(x, y, 0) = \psi_0(x, y) \quad (13)$$

This function evolution PDE makes all level sets  $\{(x, y) : \psi(x, y, t) = \text{const.}\}$  of  $\psi$  (not only the zero level) expand with normal speed  $c$ . If  $c = 1$ , it is identical to the flat circular dilation PDE (3) by equating scale with time. Thus, we can view this specific dilation PDE as a special case of the general function evolution PDE (13) where all level sets expand in a homogeneous medium with  $c = 1$ . Propagation in a heterogeneous medium with  $c = c(x, y) > 0$  will lead later to the eikonal PDE.

### 5.2 Curvature-dependent Flow

Consider a curve evolving by (10) with  $c = 1 - \varepsilon \kappa$ ,  $\varepsilon \geq 0$ . This velocity model has been studied extensively in [40, 50] for general evolution of interfaces and in [21, 22] for shape analysis in computer vision. When  $c = 1$ , the curvature  $\kappa$  evolves according to [50]

$$\kappa_t = \varepsilon \kappa_{\ell\ell} + \varepsilon \kappa^3 - \kappa^2 \quad (14)$$

When  $\varepsilon > 0$ , the front remains smooth. However, if  $\varepsilon = 0$ , then (14) becomes  $\kappa_t = -\kappa^2$  whose solution is  $\kappa(p, t) = \kappa(p, 0)/[1 + t\kappa(p, 0)]$ . Thus, when  $c = 1$ , the front's curvature will develop singularities and the front will develop corners (i.e., the curve derivatives will develop shocks – discontinuities) at finite time if the initial curvature is anywhere negative. Two ways to continue the front beyond the corners are: i) If the front is viewed as a geometric curve, then each point is advanced along the normal by a distance  $t$ , and hence a ‘swallowtail’ is formed beyond the corners by allowing the front to pass through itself. ii) If the front is viewed as the boundary separating two regions, an **entropy condition** [50] is imposed to disallow the front to pass through itself. Namely, if the front is a propagating flame, then ‘once a particle is burnt it stays burnt’ [50]. The same idea was also used in [5] to model grassfire propagation leading to the medial axis of a shape. It is equivalent to using Huyghen’s principle to construct the front as the set of points at distance  $t$  from the initial front. This can also be obtained from multiscale dilations of the initial front by disks of radii  $t > 0$ . Both the swallowtail and the entropy solutions are *weak solutions* [25]. See Fig. 2 for an example. As Fig. 2 shows, when  $\varepsilon > 0$ , motion with curvature-dependent speed has a smoothing effect. Further, the limit of the solution for the  $c = 1 - \varepsilon \kappa$  case as  $\varepsilon \downarrow 0$  is the entropy solution for the  $c = 1$  case [50].

Another important case of curve evolution is when  $c = -\kappa$ ; then,

$$\vec{X}_t = -\kappa \vec{N} = \vec{X}_{\ell\ell} \quad (15)$$

where  $\ell$  is arc length. This propagation model is known as *Euclidean geometric heat (or shortening) flow*. Smooth simple curves evolving by (15) remain smooth and simple and undergo interesting phenomena: Their perimeter shrinks as fast as possible [14]. Any convex curve remains convex and shrinks to a round point [14, 15]. Further, any non-convex curve converges first to a convex curve and from there it converges to a round point [16]. See Fig. 3 for an example. Contrast the geometric heat flow (15) with the linear heat flow

$$\vec{X}_t = \vec{X}_{pp} \iff \begin{cases} x_t = x_{pp} \\ y_t = y_{pp} \end{cases} \quad (16)$$

where the coordinate functions  $x(p, t)$  and  $y(p, t)$  satisfy the heat PDE (1) and hence are the multiscale linear convolutions of  $x(p, 0)$  and  $y(p, 0)$  with a Gaussian of variance  $2t$ .

If the function  $\psi(x, y, t)$  embeds a curve evolving by (15) as its zero level set, then it satisfies the evolution PDE

$$\psi_t = \operatorname{div}(\nabla \psi / \|\nabla \psi\|) \|\nabla \psi\| \quad (17)$$

This smooths all level sets by propagation under their mean curvature. It has many interesting properties and has been studied extensively [40, 12, 4, 50].

Solutions of the Euclidean geometric heat flow (15) are invariant with respect to the group of Euclidean transformations (rotations and translations). Extending this invariance to affine transformations creates the *affine geometric heat flow* introduced in [47]

$$\vec{X}_t = -\kappa^{1/3} \vec{N} = \vec{X}_{\alpha\alpha} \quad (18)$$

where  $\alpha$  is the affine arc length, i.e., a re-parameterization of the curve such that  $|\det(\vec{X}_\alpha, \vec{X}_{\alpha\alpha})| = 1$ . Any smooth simple non-convex curve evolving by the affine flow (18) converges to a convex one and from there to an elliptical point [47].

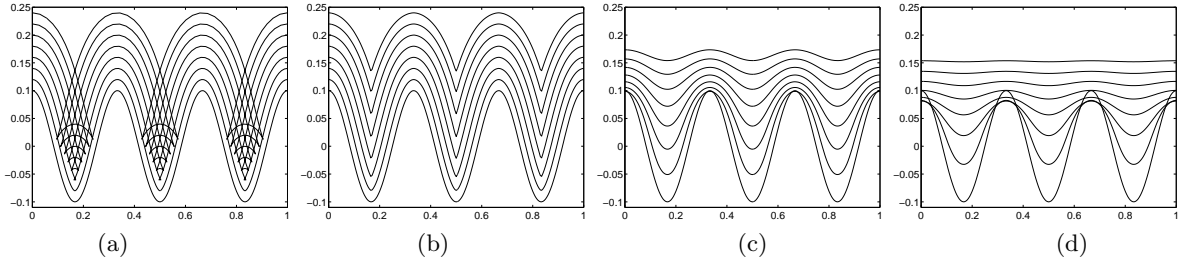


Figure 2: Evolution of the curve (signal graph)  $(-p, \cos(6\pi p)/10)$ ,  $p \in [0, 1]$ . Evolved curves are plotted from  $t = 0$  to  $t = 0.14$  at increments of 0.02. The numerical simulation for (b,c,d) is based on the Osher & Sethian algorithm with  $\Delta x = 0.005$  and  $\Delta t$  chosen small enough for stability. (a)  $c = 1$ , 'swallowtail' weak solution. (b)  $c = 1$ , entropy weak solution with  $\Delta t = 0.002$ . (c)  $c = 1 - 0.05\kappa$  with  $\Delta t = 0.0002$ . (d)  $c = 1 - 0.1\kappa$  with  $\Delta t = 0.0001$ .

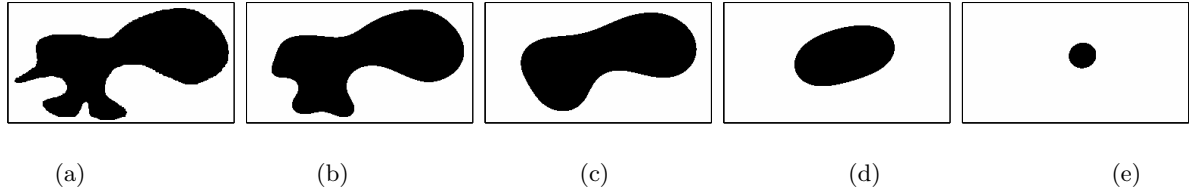


Figure 3: A nonconvex shape collapsing to a round point under curvature flow ( $c = -0.1\kappa$ ). (a) Original. (b) 500 iterations. (c) 2000 iterations. (d) 9000 iterations. (e) 14000 iterations.

### 5.3 Numerical Algorithm

The level set method for curve evolution with speeds  $c = C - \varepsilon\kappa$ , where  $C$  depends only on  $x, y$ , leads to the Hamilton-Jacobi PDE

$$\psi_t = C||\nabla\psi|| - \varepsilon\kappa||\nabla\psi|| \quad (19)$$

If  $\varepsilon = 0$ , such flows develop shocks even if the initial data are smooth. After the shock formation, the solutions must be extended in a way that respects the original motion equation in conservation form and satisfies the entropy condition. Further, it is desirable from any good discretization scheme to be highly accurate over smooth regions, reduce oscillations, and resolve shocks by confining them to a few grid points in a nonoscillatory way. By adapting the technology of conservative monotone discretization schemes for shock-producing PDEs of hyperbolic conservation laws [25], stable and shock-capturing numerical algorithms were developed in [40] for solving the above Hamilton-Jacobi PDEs. The main steps of such a first-order algorithm [40] to find an approximate solution to  $\psi_t = C||\nabla\psi||$ ,  $C = C(x, y) > 0$ , are:

Let  $\Psi_{i,j}^n$  be an estimate of  $\psi(i\Delta x, j\Delta y, n\Delta t)$  on a grid.  
 $D_x^+ = (\Psi_{i+1,j}^n - \Psi_{i,j}^n)/\Delta x$  , ,  $D_x^- = (\Psi_{i,j}^n - \Psi_{i-1,j}^n)/\Delta x$   
 $D_y^+ = (\Psi_{i,j+1}^n - \Psi_{i,j}^n)/\Delta y$  , ,  $D_y^- = (\Psi_{i,j}^n - \Psi_{i,j-1}^n)/\Delta y$   
 $F^2 = \min^2(0, D_x^-) + \max^2(0, D_x^+) + \min^2(0, D_y^-)$   
 $+ \max^2(0, D_y^+)$   
 $\Psi_{i,j}^{n+1} = \Psi_{i,j}^n + C_{i,j}|F|\Delta t$  , ,  $n = 1, 2, \dots, (T_{max}/\Delta t)$

where  $T_{max}$  is the maximum time (or scale) of interest,  $\Delta x, \Delta y$  are the spatial grid spacings,  $\Delta t$  is the time (scale) step, and  $C_{i,j} = C(i\Delta x, j\Delta y)$ . For stability [40], the space/time steps must satisfy  $(\Delta t/\Delta x + \Delta t/\Delta y)C_{i,j} \leq 0.5$ .

The dilation/erosion PDEs can be numerically solved via the above algorithm. Thus, by choosing fine grids (and possibly higher order terms) an arbitrarily low error (between signal values on the continuous plane and the discrete grid)

can be achieved in implementing morphological operations involving disks as structuring elements. This is a significant advantage of the PDE approach, as observed in [46]. Thus, curve evolution provides a geometrically better implementation of multiscale morphological operations with the disk-shaped structuring element. See Fig. 4 for an example.

If  $\varepsilon \neq 0$ , a discretization scheme for the curvature term  $\varepsilon\kappa||\nabla\psi||$  in (19) must use central difference approximations to the derivatives involved.

### 6 Nonlinear Diffusion & Directional Smoothing

To avoid the edge blurring of Gaussian scale-space, a nonlinear diffusion PDE was proposed in [41]

$$u_t = \operatorname{div}(k\nabla u) = k\nabla^2 u + \nabla k \cdot \nabla u \quad (20)$$

where  $k$  is a varying diffusion coefficient (dependent possibly on any of  $x, y, t, u, \nabla u$ ) whose purpose is to favor intraregion over interregion smoothing, i.e., to inhibit or reduce smoothing at strong edges. This can be accomplished if  $k = E(||\nabla u||)$ , and  $E$  is a smooth nonincreasing function with  $E(0) = 1$ ,  $E(r) \geq 0$ , and  $\lim_{r \rightarrow \infty} E(r) = 0$ . With such a choice for  $k$ , the diffusion will be small (large) when the edges are strong (weak), where the edge strength is measured by  $||\nabla u||$ . Typical choices of  $E$  include  $E(r) = \exp(-ar)$  and  $E(r) = a/(a + r^2)$ ,  $a > 0$ .

Two problems with the diffusion scheme (20) are the amplification of noise by the gradient and sensitivity to initial conditions for certain choices of  $g$ . These problems were solved in [11] by replacing the estimated edge strength  $||\nabla u||$  with  $||\nabla G^{(s)} * u||$ , i.e., by smoothing with a Gaussian at some fixed scale  $s$  before taking the gradient. This solution did not have a clear geometric interpretation and the stability of the model was not guaranteed as  $s \rightarrow 0$ . A further improved

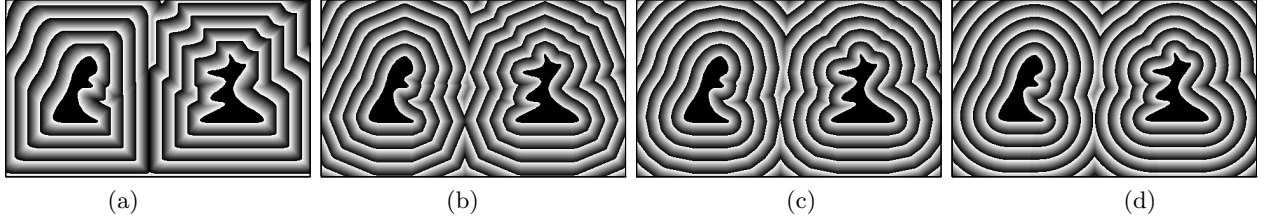


Figure 4: Distance transforms (modulo a constant) of a binary image, obtained via: (a) (1,1) chamfer metric; (b) optimal  $3 \times 3$  chamfer metric; (c) optimal  $5 \times 5$  chamfer metric; (d) curve evolution.

solution was given in [2] and its simplest form is

$$u_t = E(|\nabla G^{(s)} * u|) \operatorname{div}(\nabla u / |\nabla u|) |\nabla u| \quad (21)$$

The term  $\operatorname{div}(\nabla u / |\nabla u|) |\nabla u|$  performs a pure anisotropic diffusion by diffusing  $u$  only in the direction orthogonal to  $\nabla u$  and not all in the direction of  $\nabla u$ . The contrast term  $E(|\nabla G^{(s)} * u|)$  controls the speed of diffusion and thus enhances the edges. From the level set method of curve evolution, evolving  $u$  according to (21) propagates all its level sets with a normal speed equal to their curvature ( $-\kappa$ ) times  $E(|\nabla G^{(s)} * u|)$ .

## 7 Signal Restoration using Shock Filters

A class of nonlinear hyperbolic PDEs of the wave type was proposed in [39] to deblur images and/or enhance their contrast by edge sharpening. For 1D images such a PDE is

$$u_t = -|u_x| F(u_{xx}) \quad (22)$$

where  $F$  is a Lipschitz continuous function satisfying  $F(0) = 0$  and  $F(r)r \geq 0$ . Starting at  $t = 0$ , with the blurred image  $u(x, 0) = f(x)$  as the initial data, and running the PDE until some time  $t$  yields a filtered image  $u(x, t)$ . Its goal is to restore blurred discontinuities (edges) sharply, accurately and in a nonoscillatory way. Steady state is reached as  $t \rightarrow \infty$ . This PDE model develops shocks at zero crossings of  $u_{xx}$ . Consider now a special case of (22) with  $F(r) = \operatorname{sign}(r)$ :

$$u_t = -|u_x| \operatorname{sign}(u_{xx}) \quad (23)$$

At points  $x$  where  $u_{xx} > 0$ , this PDE shifts parts of the graph of  $u(x, t)$  with positive (negative) slope to the right (left) but does not move the extrema or inflection points. If  $u_{xx} < 0$  the direction of propagation reverses. Thus, over convex regions ( $u_{xx} > 0$ ) it acts as a 1D erosion PDE  $u_t = -|u_x|$  which models multiscale flat erosion of  $f(x)$  by the horizontal line segment  $[-t, t]$ , whereas over concave regions ( $u_{xx} < 0$ ) it acts as a 1D dilation PDE  $u_t = |u_x|$  which models multiscale flat dilation of  $f(x)$  by the same segment. For certain piecewise-constant signals blurred via linear convolution with finite-window smooth tapered symmetric kernels, the shock filtering  $u(x, 0) \mapsto u(x, \infty)$  can recover the original signal and thus achieve an exact deconvolution [39].

To produce a shock-capturing numerical method for solving (22), the following discretization scheme was proposed in [39] ( $U_i^n$  is an approximation of  $u(x, t)$  on a grid  $(i\Delta x, n\Delta t)$ ):

$$\begin{aligned} U_i^{n+1} = U_i^n & - \Delta t (F_i^n)^+ \sqrt{((D_i^-)^+)^2 + ((D_i^+)^-)^2} \\ & - \Delta t (F_i^n)^- \sqrt{((D_i^-)^-)^2 + ((D_i^+)^+)^2} \end{aligned} \quad (24)$$

where  $F_i^n = F(U_i^n)$ ,  $D_i^\pm = \pm(U_{i\pm 1}^n - U_i^n)/\Delta x$ ,  $r^+ = \max(0, r)$ , and  $r^- = \min(0, r)$ . For stability,  $\sup_i (\Delta t/\Delta x) F_i^n \leq 0.5$ . When  $n \rightarrow \infty$  the above scheme converges to a fixed point. An example of its action is shown in Fig. 5.

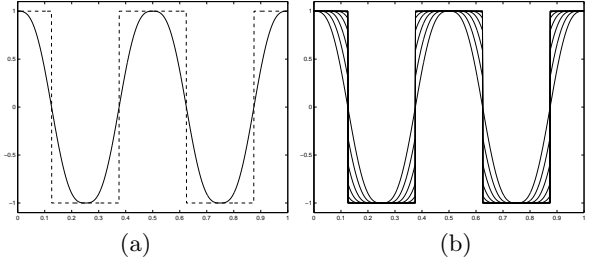


Figure 5: (a) Original periodic signal (dashed line) and its blurring  $u(x, 0)$  (solid line) via convolution with a finite positive symmetric tapered impulse response. (b) Evolutions  $u(x, t)$  from  $t = 0$  until convergence (reached at 371 iterations), plotted at time increments of 0.02.  $\Delta x = 0.001$ ,  $\Delta t = 0.0005$ .

The edge sharpening produced by (24) is almost identical to that of iterating the following discrete morphological operator

$$U_i^{n+1} = \begin{cases} d = \max(U_{i-1}^n, U_i^n, U_{i+1}^n), & U_i^n \geq (d+e)/2 \\ e = \min(U_{i-1}^n, U_i^n, U_{i+1}^n), & U_i^n < (d+e)/2 \end{cases} \quad (25)$$

At each  $i$ , the output value for the next iteration toggles between a discrete flat dilation  $d$  (3-point moving local max) and a flat erosion  $e$  (3-point moving local min) of the previous iteration according to which is closer to the central initial value  $U_i^n$ . Now, both schemes (24) and (25) converge to the same fixed point. Further, we have found that, if  $\Delta t = \Delta x$ , then (24) and (25) produce identical outputs at each iteration step.

Extensions of the PDE (22) for 2D image deblurring has also been developed in [39] by replacing  $|u_x|$  with  $|\nabla u|$  and  $u_{xx}$  with  $\nabla^2 u$ .

The discretization scheme (24) preserves the variation, size and location of extrema. However, this has undesirable consequences in the presence of noise. Thus, it cannot remove ‘salt-pepper’ noise and in general it may enhance others types of noise in the blurred image. To reduce this noise sensitivity, an improved version was proposed in [3]:

$$u_t = -F_2(G^{(s)} * u_{xx}, G^{(s)} * u_x) u_x \quad (26)$$

where  $F_2$  must satisfy  $F_2(p, q)pq \geq 0$ . For example,  $F_2(p, q) = \operatorname{sign}(p)\operatorname{sign}(q)$ . The smoothing of the derivatives

by convolving with Gaussians adds some robustness to this shock filtering.

## 8 Eikonal PDE

Many tasks for extracting information from visible images have been related to optics and wave propagation via the *eikonal PDE* [7]

$$\|\nabla\phi(x, y)\| = \eta(x, y) \quad (27)$$

Its solution  $\phi(x, y)$  can provide shape from shading, analog contour-based halftoning, and topographic segmentation of an image  $f(x, y)$  by choosing the refractive index field  $\eta(x, y)$  to be an appropriate function of the image [48, 18, 53, 42, 23, 38, 29]. The eikonal PDE can be seen as a stationary formulation of the embedding function evolution PDE (13) with positive speed  $c(x, y) = c_0/\eta(x, y) > 0$ . Namely [40, 13], if  $T(x, y)$  is the time at which the zero level of  $\psi(x, y, t)$  crosses  $(x, y)$ , then  $\|\nabla T\| = 1/c$ . Setting  $\phi = c_0 T$  leads to the eikonal.

The solution of the eikonal PDE can be viewed as a *weighted distance function* [26, 53, 44, 23, 29] between a point  $(x, y)$  and the sources along a path of minimal optical length. The optical length of any path is obtained by integrating the refractive index field  $\eta(x, y)$  along this path and is proportional to the time required for light to travel this path. Thus, we can view the solution  $\phi(x, y)$  of the eikonal as a **gray-weighted distance transform (GWDT)** whose values at each pixel give the minimum distance from the light sources weighted by the gray values of the refractive index field. Next we outline two ways of solving the eikonal PDE.

### 8.1 GWDT based on Chamfer Metrics

Let a sampled positive image be viewed as a discrete refractive index field  $\eta[x, y]$ . A discrete GWDT of this image (which is an approximation [53] to the solution of the eikonal PDE  $\|\nabla u\| = \eta$ ) can be obtained via the following min-sum recursive difference equation

$$\begin{aligned} U_n[x, y] = \min\{U_n[x - 1, y] + a\eta[x, y], \\ U_n[x, y - 1] + a\eta[x, y], U_n[x - 1, y - 1] + b\eta[x, y], \\ U_n[x + 1, y - 1] + b\eta[x, y], U_{n-1}[x, y]\} \end{aligned}$$

where  $U_0[x, y]$  is set equal to 0 if  $[x, y]$  belongs to a wave source point or  $+\infty$  otherwise. The constants  $a$  and  $b$  are the local distance steps by which the chamfer distances are propagated within a  $3 \times 3$  neighborhood. The above recursive equation is run over the whole image in forward and backward order, iteratively ( $n = 1, 2, 3, \dots$ ) until stability. At convergence,  $U_\infty$  is the GWDT of  $f$ . The above is a sequential implementation of the GWDT. There are also other faster implementations using queues [53, 35, 36].

The propagation of the local distances  $(a, b)$  starts at the wave sources and moves with speed  $c(x, y) = c_0/\eta[x, y]$ . To improve the GWDT approximation to the eikonal's solution, one can optimize  $(a, b)$ . Using a neighborhood larger than  $5 \times 5$  can further reduce the approximation error but at the cost of an even slower implementation. However, larger neighborhood masks cannot be used with GWDTs because they give erroneous results since the large masks can bridge over a thin line that separates two segmentation regions. Overall, this chamfer metric approach to GWDT is fast and easy to implement, but due to the required small neighborhoods is not isotropic and cannot achieve high accuracy.

### 8.2 GWDT based on Curve Evolution

In this approach, at time  $t = 0$  the boundary of each source is modeled as a curve  $\gamma(0)$  which is then propagated with normal speed  $c(x, y) = c_0/\eta(x, y)$ . The propagating curve  $\gamma(t)$  is embedded as the zero level set of a function  $\psi(x, y, t)$ , where  $\psi(x, y, 0) = \psi_0(x, y)$  is the signed (positive in the curve interior) distance from  $\gamma(0)$ . The function  $\psi$  evolves according to the PDE

$$\psi_t = c(x, y)\|\nabla\psi\| \quad (28)$$

which corresponds to curve evolution in a heterogeneous medium with position-dependent speed  $c > 0$ , or equivalently to a successive front dilation by disks with position-varying radii  $c(x, y)dt$ . This is a time-dependent formulation of the eikonal PDE [40, 13]. It is solved via the numerical algorithm of [40]. The value of the resulting GWDT at any pixel  $(x, y)$  of the image is the time it takes for the evolving curve to reach this pixel, i.e. the smallest  $t$  such that  $\psi(x, y, t) \geq 0$ . This continuous approach to GWDT can achieve sub-pixel accuracy, as investigated in [23]. To reduce the computational complexity of the above curve evolution algorithm, in our joint work [30] we have developed a queue-based implementation of the fast marching level set methods of [50, 27] adapted to computing GWDTs in case of multiple sources where triple points develop at the collision of several wavefronts.

### 8.3 Ray Tracing

Ray tracing in optical media is also modeled via the eikonal. In Fig. 6, a plane (2D optical medium) is divided into two regions of different refractive indexes, and the path of minimum optical length (least propagation time) is to be found between two points in these regions. There we see that, the GWDT based on curve evolution gives a better approximation of the true path of light than the GWDTs based on the discrete (chamfer) distance transforms.

### 8.4 Gridless Halftoning via Eikonal PDE

Inspired by the use in [48] of the eikonal function's contour lines for visually perceiving an intensity image  $I(x, y)$ , the work in [53] and especially in [42] attempts to solve the PDE  $\|\nabla\phi(x, y)\| = \text{const} - I(x, y)$  and create a binary *gridless* halftone version of  $I(x, y)$  as the union of the isolevel curves of the eikonal function  $\phi(x, y)$ . The larger the intensity value  $I(x, y)$ , the smaller the local density of these contour lines in the vicinity of  $(x, y)$ . This eikonal PDE approach to gridless halftoning is indeed very promising and can simulate various artistic effects, as shown in Fig. 7. There we also see that the curve evolution GWDT gives a smoother halftoning of the image than the GWDTs based on chamfer metrics.

### 8.5 Watershed Segmentation via Eikonal

A powerful morphological approach to *image segmentation* is the *watershed* [37, 54] which transforms an image  $f(x, y)$  to the crest lines separating adjacent catchment basins that surround regional minima or other 'marker' sets of feature points. In [35, 36, 38] it has been established that (in the continuous domain and assuming that the image is smooth and has isolated critical points) the continuous watershed is equivalent to finding a skeleton by influence zones with respect to a weighted distance function that uses the (one-point) regional minima of the image as sources and  $\|\nabla f\|$

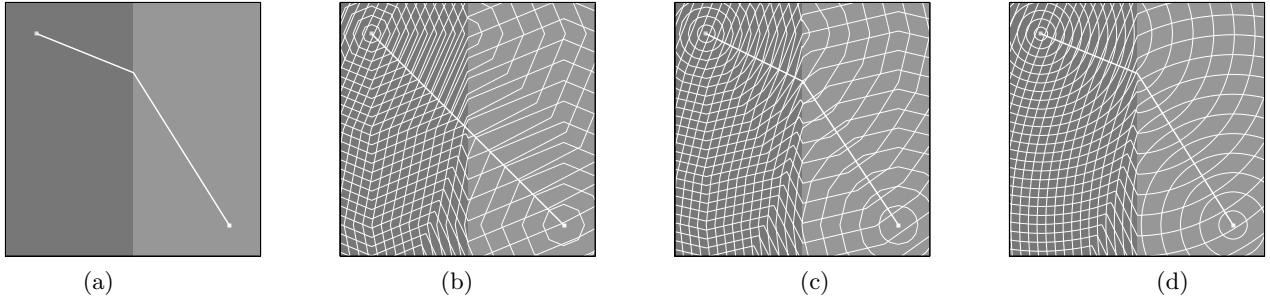


Figure 6: (a) Image of an optical medium consisting of two areas of different refractive index and the correct path of the light ray (from Snell's law) between two points. The paths in (b,c,d) are found by using GWDT based on: (b) optimal chamfer metric with  $3 \times 3$  neighborhood; (c) optimal chamfer metric with  $5 \times 5$  neighborhood; (d) curve evolution. In (b),(c),(d) the thin light contours show the wavefronts propagating from the two source points according to the various metrics.



Figure 7: Gridless halftoning of the CAMERAMAN image from 100 contour lines of GWDTs obtained via: (a)  $(1,1)$  chamfer metric; (b) optimal  $3 \times 3$  chamfer metric; (c) optimal  $5 \times 5$  chamfer metric; (d) curve evolution. In (a,b,c,d) the light source was at the top left corner.

as the field of indices. (If other markers different than the minima are to be used as sources, then the homotopy of the function must be modified via morphological reconstruction to impose these markers as the only minima.) Hence, it has been proposed in [36, 38] to use existing efficient digital watershed algorithms for finding the solution to the eikonal.

In our joint work [30] we solve the above eikonal PDE model of watershed segmentation of an image-related function  $f$  by finding a GWDT via curve evolution (28) where the speed is  $c \propto 1/\|\nabla f\|$ . Further we compare the results of this new segmentation to the digital watershed algorithm via flooding [54] and to the eikonal approach solved via a discrete GWDT based on chamfer metrics [53, 36]. In all three approaches, robust features are extracted first as markers of the regions, and the original image  $I$  is transformed to another function  $f$  by smoothing via alternating open/closing at multiple scales, taking the gradient magnitude of the filtered image, and changing (via morphological reconstruction) the homotopy of the gradient image so that its only minima occur at the markers. The segmentation is done on the final outcome  $f$  of the above processing.

In the standard digital watershed algorithm [54, 37], the flooding at each level is achieved by a planar distance propagation that uses the chess-board metric. This kind of distance propagation is non-isotropic and could give wrong results, particularly for images with large plateaus, as we found experimentally. Eikonal segmentation using GWDTs based on chamfer metrics improves this situation a little but not entirely. In contrast, for images with large plateaus/regions, segmentation via the eikonal PDE and

curve evolution GWDT gives results close to ideal. As Fig. 8 shows, compared on a test image that is difficult (because expanding wavefronts meet watershed lines at many angles ranging from being perpendicular to almost parallel), our continuous segmentation approach based on the eikonal PDE and curve evolution outperforms the discrete segmentation results (using either the digital watershed flooding algorithm or chamfer metric GWDTs). However, some real images, as in Fig. 9, may not contain many plateaus or only large regions, in which cases the digital watershed flooding algorithm may give comparable results (or slightly better for thin elongated regions) than the eikonal PDE approach. In our on-going work, we are currently continuing the detailed comparison of these two approaches.

## Acknowledgement

I wish to thank Akmal Butt at Georgia Tech for producing the image figures and for insightful discussions.

## References

- [1] L. Alvarez, F. Guichard, P.L. Lions, and J.M. Morel, “Axiomatization et nouveaux operateurs de la morphologie mathematique”, *C. R. Acad. Sci. Paris*, pp. 265–268, t.315, Serie I, 1992.
- [2] L. Alvarez, P.-L. Lions, and J.-M. Morel, “Image Selective Smoothing and Edge Detection by Nonlinear Diffusion. II”, *SIAM J. Numer. Anal.*, vol. 29, pp. 845–866, June 1992.

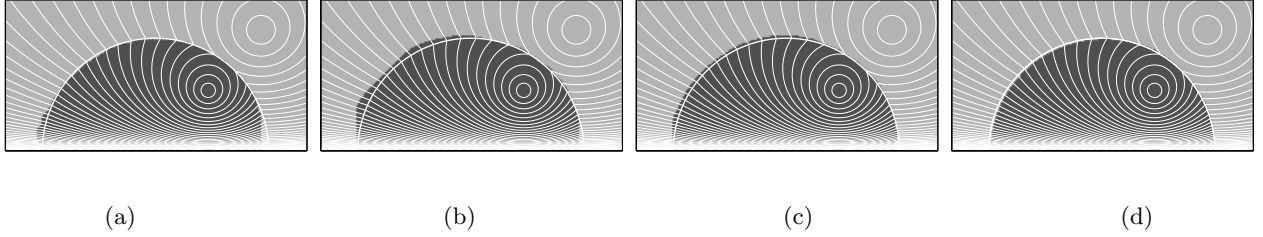


Figure 8: The TEST image is the minimum of two potential functions. Its contour plot (thin bright curves) is superimposed on all segmentation results. Markers are the two source points of the potential functions. Segmentation results based on: (a) Digital watershed flooding algorithm. (b) GDWT based on optimal  $3 \times 3$  chamfer metric. (c) GDWT based on optimal  $5 \times 5$  chamfer metric. (d) GDWT based on curve evolution. (The thick bright curve shows the correct segmentation.)



Figure 9: (a) Original CAMERAMAN image with markers placed within desired regions. (b) Gradient magnitude of filtered image. (c) Segmentation result (superimposed on original) from digital watershed flooding algorithm. (d) Segmentation from eikonal PDE and curve evolution GWDT.

- [3] L. Alvarez and L. Mazorra, "Signal and Image Restoration using Shock Filters and Anisotropic Diffusion", *SIAM J. Numer. Anal.*, vol. 31, no. 2, pp. 590–605, Apr. 1994.
- [4] L. Alvarez and J.M. Morel, "Formalization and computational aspects of image analysis", *Acta Numerica*, pp. 1–59, 1994.
- [5] H. Blum, "Biological shape and visual science (part I)", *J. Theor. Biol.*, vol. 38, pp. 205–287, 1973.
- [6] G. Borgefors, "Distance Transformations in Digital Images", *Comp. Vision, Graphics, Image Process.*, 34, pp. 344–371, 1986.
- [7] M. Born and E. Wolf, *Principles of Optics*, Pergamon Press, Oxford, England, 1959 (1987 edition).
- [8] R. W. Brockett and P. Maragos, "Evolution Equations for Continuous-Scale Morphology", *Proc. IEEE Int'l Conf. Acoust., Speech, Signal Processing*, San Francisco, CA, March 1992.
- [9] R. Brockett and P. Maragos, "Evolution Equations for Continuous-Scale Morphological Filtering", *IEEE Trans. Signal Processing*, vol. 42, pp. 3377–3386, Dec. 1994.
- [10] M. A. Butt and P. Maragos. "Optimal Design of Chamfer Distance Transforms", *IEEE Trans. Image Processing*, to appear.
- [11] F. Catte, T. Coll, P.-L. Lions, and J.-M. Morel, "Image Selective Smoothing and Edge Detection by Nonlinear Diffusion", *SIAM J. Numer. Anal.*, vol. 29, pp. 182–193, 1992.
- [12] L. C. Evans and J. Spruck, "Motion of Level Sets by Mean Curvature. I", *J. Diff. Geom.*, vol. 33, pp. 635–681, 1991.
- [13] M. Falcone, T. Giorgi and P. Loreti, "Level Sets of Viscosity Solutions: Some Applications to Fronts and rendez-vous Problems", *SIAM J. Appl. Math.*, vol. 54, pp. 1335–1354, Oct. 1994.
- [14] M. E. Gage, "Curve Shortening Makes Convex Curves Circular", *Invent. Math.*, vol. 76, pp. 357–364, 1984.
- [15] M. Gage and R. S. Hamilton, "The Heat Equation Shrinking Convex Plane Curves", *J. Diff. Geom.*, vol. 23, pp. 69–96, 1986.
- [16] M. A. Grayson, "The Heat Equation Shrinks Embedded Plane Curves to Round Points", *J. Diff. Geom.*, vol. 26, pp. 285–314, 1987.
- [17] H.J.A.M. Heijmans and P. Maragos, "Lattice Calculus and the Morphological Slope Transform", *Signal Processing*, vol. 59, pp. 17–42, 1997.
- [18] B.K.P. Horn, *Robot Vision*, MIT Press, Cambridge, MA, 1986.
- [19] Special Session on "Nonlinear Dynamics for Image Processing", *Proc. Int'l Conf. Image Processing*, Austin, TX, Nov. 1994.
- [20] A. K. Jain, "Partial Differential Equations and Finite Difference Methods in Image Processing, Part I–Image Representation", *J. Optimiz. Theory & Appl.*, vol. 233(1), pp. 65–91, Sep. 1977.

- [21] B. Kimia, A. Tannenbaum, and S. Zucker, "Toward a Computational Theory of Shape: An Overview", Proc. European Conf. on Comp. Vision, France, April 1990.
- [22] B. Kimia, A. Tannenbaum, and S. Zucker, "On the Evolution of Curves via a Function of Curvature. I. The Classical Case", *J. Math. Anal. Appl.*, 163, p. 438-458, 1992.
- [23] R. Kimmel, N. Kiryati, and A. M. Bruckstein, "Sub-Pixel Distance Maps and Weighted Distance Transforms", *J. Math. Imaging & Vision*, 6:223-233, 1996.
- [24] J. J. Koenderink, "The Structure of Images", *Biol. Cybern.*, 50, pp. 363-370, 1984.
- [25] P. D. Lax, *Hyperbolic Systems of Conservation Laws and the Mathematical Theory of Shock Waves*, SIAM, Philadelphia, PA, 1973.
- [26] G. Levi and U. Montanari, "A Grey-Weighted Skeleton", *Information and Control*, 17, pp.62-91, 1970.
- [27] R. Malladi, J. A. Sethian, and B. C. Vemuri, "A Fast Level Set Based Algorithm for Topology-Independent Shape Modeling", *J. Math. Imaging and Vision*, 6, pp. 269-289, 1996.
- [28] P. Maragos, "Pattern Spectrum and Multiscale Shape Representation", *IEEE Trans. Pattern Anal. Mach. Intellig.*, vol. 11, pp. 701-716, July 1989.
- [29] P. Maragos, "Differential Morphology and Image Processing", *IEEE Trans. Image Processing*, vol. 78, pp. 922-937, June 1996.
- [30] P. Maragos and M. A. Butt, "Advances in Differential Morphology: Image Segmentation via Eikonal PDE & Curve Evolution and Reconstruction via Constrained Dilatation Flow", *Proc. Int'l Symp. Mathematical Morphology*, Amsterdam, June 1998.
- [31] P. Maragos and R. W. Schafer, "Morphological Systems for Multidimensional Signal Processing", *Proc. IEEE*, vol. 78, pp. 690-710, Apr. 1990.
- [32] D. Marr, *Vision*, Freeman, San Francisco, 1982.
- [33] G. Matheron, *Random Sets and Integral Geometry*, Wiley, New York, 1975.
- [34] J. Mattioli, "Differential Relations of Morphological Operators", *Proc. 1st Int'l Workshop on Math. Morphology and its Application to Signal Processing*, Barcelona, Spain, May 1993.
- [35] F. Meyer, "Integrals and Gradients of Images", *Proc. SPIE vol. 1769: Image Algebra and Morphological Image Processing III*, pp.200-211, 1992.
- [36] F. Meyer, "Topographic Distance and Watershed Lines", *Signal Processing*, 38, pp. 113-125, 1994.
- [37] F. Meyer and S. Beucher, "Morphological Segmentation", *J. Visual Commun. Image Representation*, 1(1):21-45, 1990.
- [38] L. Najman and M. Schmitt, "Watershed of a Continuous Function", *Signal Processing*, vol. 38, pp. 99-112, July 1994.
- [39] S. Osher and L. I. Rudin, "Feature-Oriented Image Enhancement Using Shock Filters", *SIAM J. Numer. Anal.*, vol. 27, no. 4, pp. 919-940, Aug. 1990.
- [40] S. Osher and J. Sethian, "Fronts Propagating with Curvature-Dependent Speed: Algorithms Based on Hamilton-Jacobi Formulations", *J. Comput. Physics*, 79, pp. 12-49, 1988.
- [41] P. Perona and J. Malik, "Scale-Space and Edge Detection Using Anisotropic Diffusion", *IEEE Trans. Pattern Anal. Mach. Intellig.*, vol. 12, pp. 629-639, July 1990.
- [42] Y. Pnueli and A. M. Bruckstein, "DigiDürer - a digital engraving system", *The Visual Computer*, 10, pp. 277-292, 1994.
- [43] A. Rosenfeld and J. L. Pfaltz, "Sequential Operations in Digital Picture Processing", *J. ACM*, 13, pp. 471-494, Oct. 1966.
- [44] E. Rouy and A. Tourin, "A Viscosity Solutions Approach to Shape from Shading", *SIAM J. Numer. Anal.*, vol. 29 (3), pp. 867-884, June 1992.
- [45] P. Salembier and J. Serra, "Morphological Multiscale Image Segmentation", in *Visual Communications and Image Processing*, P. Maragos, Ed., Proc. SPIE vol.1818, pp. 620-631, 1992.
- [46] G. Sapiro, R. Kimmel, D. Shaked, B. Kimia, and A. Bruckstein, "Implementing Continuous-scale Morphology via Curve Evolution", *Pattern Recognition*, 26(9), pp. 1363-1372, 1993.
- [47] G. Sapiro and A. Tannenbaum, "Affine Invariant Scale-Space", *Int'l J. Comp. Vision*, 11(1), pp. 25-44, 1993.
- [48] M. Schröder, "The Eikonal Equation", *Math. Intelligencer*, vol. 1, pp. 36-37, 1983.
- [49] J. Serra, *Image Analysis and Mathematical Morphology*, Acad. Press, NY, 1982.
- [50] J. A. Sethian, *Level Set Methods*, Cambridge Univ. Press, 1996.
- [51] R. van der Boomgaard, *Mathematical Morphology: Extensions towards Computer Vision*, Ph.D. Thesis, Univ. of Amsterdam, 1992.
- [52] R. van der Boomgaard and A. Smeulders, "The Morphological Structure of Images: The Differential Equations of Morphological Scale-Space", *IEEE Trans. Pattern Anal. Mach. Intellig.*, vol. 16, pp.1101-1113, Nov. 1994.
- [53] P. Verbeek and B. Verwer, "Shading from shape, the eikonal equation solved by grey-weighted distance transform", *Pattern Recogn. Lett.*, 11:618-690, 1990.
- [54] L. Vincent and P. Soille, "Watershed In Digital Spaces: An Efficient Algorithm Based On Immersion Simulations", *IEEE Trans. Pattern Anal. Mach. Intellig.*, vol. 13, pp. 583-598, June 1991.
- [55] A. P. Witkin, "Scale-Space Filtering", *Proc. Int'l Joint Conf. Artif. Intellig.*, Karlsruhe, Germany, 1983.